International Journal of Automotive Technology, Vol. 21, No. 0, pp. 1–10 (2020)
DOI 10.1007/s12239–018–

pISSN 1229–9138/ eISSN 1976–3832

MODEL PREDICTIVE CONTROL OF AN ALL-WHEEL DRIVE VEHICLE CONSIDERING INPUT AND STATE CONSTRAINTS

Hojin Jung[1)], Beomjoon Pyun[2)] and Seibum Choi[1)*]

[1)]Department of Mechanical Engineering, KAIST, Daejeon 34141, Korea
[2)]Driving & Safety System R&D Center, Korea Automotive Technology Institute, 303 Pungse-ro, Pungse-myeon, Dongnam-gu, Cheonan-si, Chungnam 31214, Korea

(Received 25 June 2018; Revised 20 May 2019; Accepted 1 July 2019)

ABSTRACT–This paper suggests a novel model-based control scheme for an all-wheel drive (AWD) vehicle. Using transfer case, AWD system is able to transfer the engine torque to all the wheels mechanically, helping the vehicle to maintain traction on a slippery road or to climb a hill. Recently, an active type AWD system that is able to control the torque transmitted through transfer case continuously by the aid of electronic clutch actuator has become popular. In order to realize preemptive operation which is necessary property for AWD system while simultaneously considering states and input constraints which is originated from mechanical and physical characteristics, this paper adopted model predictive control (MPC) concept. The proposed MPC-based controller was designed by using planar full-car model that is based on tire force and motion states, which represents the direct relationship between these states and control input. Therefore, the planar full-car model contributed the suggested controller to follow standard MPC design process. The target states of longitudinal wheel slip and yaw rate, which have commonly been adopted in previous studies, were selected for practical concerns. The advantages of the suggested MPC-based controller that is designed especially for an AWD system were validated by conducting simulations through a Simulink-CarSim-based AWD vehicle model.

KEY WORDS : All-wheel drive, Transfer case, Vehicle dynamics control, Model predictive control, Constrained system

NOMENCLATURE

v_x : longitudinal velocity, m/s
v_y : lateral velocity, m/s
γ : yaw rate, rad/s
ω_i : wheel angular velocity at each wheel, rad/s
m : vehicle mass, kg
I_z : moment of inertia about yaw axis, kg m^2
δ_1 : left wheel steer angle, rad
δ_2 : right wheel steer angle, rad
t_w : half of vehicle track width, m
l_f : distance from front axle to the center of gravity, m
l_r : distance from rear axle to the center of gravity, m
ρ_{air} : density of air, kg/m^3
C_d : drag coefficient, -
A : vehicle front cross sectional area, m^2
L : wheel base length, m
h_{cg} : height from ground to center of gravity, m
R_r : rolling resistance, -
R_e : effective radius of wheel, m
r_c : effective radius of transfer case clutch, m
μ : road friction coefficient, -
σ : relaxation length, m
C_α : cornering stiffness, N/rad
K_L : lateral stiffness, N/m
K_D : distortion stiffness, Nm/rad
T_t : transmission output torque, Nm
T_b : braking torque, Nm

*Corresponding author. e-mail: sbchoi@kaist.ac.kr

1. INTRODUCTION

Over the past few years, several types of vehicle dynamics control systems have been consistently developed to meet the increasing demand of vehicle safety and performance (Choi, 2008; Yoon, 2009; Choi and Choi, 2014; Kim *et al*., 2015). Among them, all-wheel drive (AWD) systems, which transfer the driving torque through the transfer case to all wheels, have proven effective for improving both vehicle performance in aspects of cost and benefit, and, thus the market share of AWD vehicles has steadily increased (Williams, 2006). Unlike the vehicle dynamics control systems, e.g., antilock brake system (ABS) and electronic stability control (ESC), the activation of an AWD system does not cause driver discomfort because it does not generate braking torque. Therefore, the AWD system is activated first among other vehicle dynamics systems when unstable or undesirable motions are detected, and taking advantage of the AWD system when it is needed can improve the vehicle's overall performance.

One type of active AWD system, a transfer case with multiple wet-clutches and an electro-hydraulic actuator, has two characteristics. First, the wet clutch system can endure clutch slip for a certain amount of time, which occurs between the fully lock-up and fully disengaged states. Therefore, an AWD vehicle equipped with this type of transfer case can determine the amount of torque that is distributed between the main-drive shaft and sub-drive shaft at ratios from 0 : 100 to 50 : 50. Second, as compared with a selective four-wheel drive (4WD) system, which is controlled manually by the driver, the electro-hydraulic actuator can determine the exact amount of transfer case engagement force automatically by constantly monitoring the vehicle states. Variable torque distribution in AWD vehicle can drastically change the motion of the vehicle in many different situations. Therefore, a model-based controller for an AWD system should be designed so that the vehicle can fully realize the advantages of the active type AWD system.

There can be two types of constraints in an AWD vehicle. First is the input constraint. In contradiction with a vehicle that is equipped with an in-wheel motor, a vehicle that is equipped with a transfer case has constrained amount of driving torque in sub-drive shaft, which is due to both the intrinsic hardware structure and the transmission output torque. Second is the state constraint. In a vehicle dynamics model, some vehicle states, e.g., yaw rate and tire force are constrained by physical factors.

There have been several studies concerning controller design for several types of AWD vehicle. Osborn and Shim (2006) suggested a map based control of in-wheel motor vehicle using matrix that represents relationship between input and output parameters. Croft-White and Harrison (2006) proposed a torque vectoring control scheme for an AWD vehicle that applies sideslip angle minimization strategy. Kim *et al*. (2015) suggested AWD and torque vectoring controller that distributes driving torque while accomplishing the least generation of additional of traction force. Jung and Choi (2016) proposed PID controller for AWD vehicle toward the error over saturation point of slip ratio and sideslip angle. However, these previous efforts did not take advantage of AWD vehicle dynamic model and also did not consider the constraints that exist in an AWD vehicle systemically.

Model predictive control (MPC) has been proven to be an effective method (Camacho and Bordons, 2007; Borrelli *et al.*, 2017), to address the aforementioned issue, and has been adopted in other studies (Choi and Choi, 2016; Jalali *et al*., 2017) because the MPC algorithm can calculate the optimal control input that minimizes the quadratic cost function, while simultaneously considering the system constraints. It is commonly understood that an AWD system can improve longitudinal acceleration performance on off-road, slippery road, and hilly road. However, the AWD system also helps the vehicle to provide a stable response in the lateral direction. This paper focuses on an AWD controller that enhances both longitudinal acceleration performance and lateral stability of vehicle.

Most previous vehicle chassis controllers were developed based on a bicycle model (Nam *et al*., 2012; Choi and Choi, 2014). However, the bicycle model cannot represent the direct relationship between the AWD clutch engagement force and the vehicle motion states, making it inappropriate to apply in an AWD controller. To design a model-based controller, this study adopted a planar full-car model that represented the direct relationship between the transfer case engagement force and motion states. Although there have been several approaches for selecting multiple target states in order to improve performance of vehicle dynamics controller, only the basic targets of vehicle longitudinal slip ratio and yaw rate, were used because the main purpose of this study was to design a model-based controller that would be practical and immediately applicable without additional sensors.

This paper is organized as follows: The vehicle model used for the MPC formulation are introduced in the second section. Selecting the target states and defining their desired values are described in the third section. The fourth section introduces the state-space form of vehicle model that was used for the controller design. In the fifth section, the system constraints that exist in the model are discussed. In the sixth section, the MPC algorithm for determining AWD control input is developed. The validation of the suggested controller, using the vehicle dynamics software CarSim, is detailed in the seventh section.

2. VEHICLE MODELS

This section introduces the vehicle model that will be used in the model-based controller and which helps to predict the future vehicle behavior.

2.1. Vehicle Motion Dynamics

Figure 1 illustrates the planar vehicle model, which

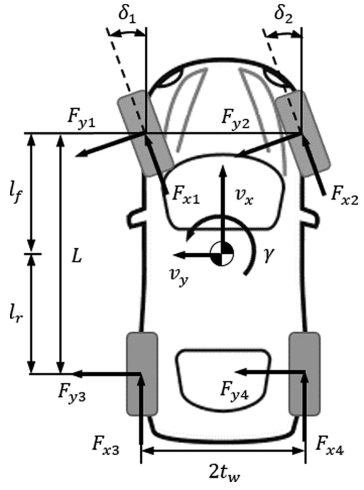

Figure 1. Planar full-car dynamic model.

includes several vehicle motion states and tire forces. Following the information in Figure 1, the equations governing the vehicle planar motion are as follows:

$$m\dot{v}_x = F_{x1}\cos(\delta_1) + F_{x2}\cos(\delta_2) - F_{y1}\sin(\delta_1) - \cdots F_{y2}\sin(\delta_2) + F_{x3} + F_{x4} - \frac{1}{2}\rho_{air} C_d A v_x^2 + m v_y \gamma \quad (1)$$

$$m\dot{v}_y = F_{x1}\sin(\delta_1) + F_{x2}\sin(\delta_2) + F_{y1}\cos(\delta_1) + \cdots F_{y2}\cos(\delta_2) + F_{y3} + F_{y4} - m v_x \gamma \quad (2)$$

$$I_z\dot{\gamma} = l_f\{F_{x1}\sin(\delta_1) + F_{x2}\sin(\delta_2) + F_{y1}\cos(\delta_1) + \cdots F_{y2}\cos(\delta_2)\} + t_w\{-F_{x1}\cos(\delta_1) + F_{x2}\cos(\delta_2) + \cdots F_{y1}\sin(\delta_1) - F_{y2}\sin(\delta_2) - F_{x3} + F_{x4}\} - l_r(F_{y3} + F_{y4}) \quad (3)$$

where v_x, v_y, and γ are the longitudinal velocity, lateral velocity, and yaw rate, respectively, at the vehicle's center of gravity (CG). F_x, F_y, δ, ρ_{air}, C_d, A, t_w, l_f, l_r, m, and I_z are the longitudinal tire force, lateral tire force, wheel steering angle, density of air, coefficient of air drag, front cross-sectional area, half track width, distance from the front axle to the vehicle's CG, distance from the rear axle to the vehicle's CG, total vehicle mass, and vehicle moment of yaw inertia, respectively. Subscript 1, 2, 3, 4 represent the front left, front right, rear left, and rear right each.

2.2. Vehicle Wheel Dynamics

The wheel dynamics model is important for an AWD vehicle because it includes a term for clutch engagement force that can be the control input for the AWD controller. Referring to the wheel dynamic model introduced by Rajamani (2012), the dynamic equation of motion for the wheel can be modified as follows:

$$I_w\dot{\omega}_i = r_c F_c \mu_c \frac{i_f}{2} - T_{bi} - R_e F_{xi} - R_e R_r F_{zi},\ i = 1, 2 \quad (4)$$

$$I_w\dot{\omega}_i = (T_t - r_c F_c \mu_c)\frac{i_r}{2} - T_{bi} - R_e F_{xi} - R_e R_r F_{zi},\ i = 3, 4 \quad (5)$$

where ω_i, T_t, i_f, i_r, T_{bi}, R_{ri}, and F_{zi} are the wheel angular velocity at each wheel, transmission output torque that can be easily obtained from the controller area network (CAN) signal of engine torque and the gear ratio, front final reduction gear ratio, rear final reduction gear ratio, braking torque, rolling resistance, and vertical load at each wheel, respectively. I_w and R_e are the wheel moment of inertia and effective wheel radius, respectively.

However, (4) and (5) are valid only when the transfer case clutch is in the slipping state. In the situation where the transfer case clutch is in lock-up state, the wheel driving torque is no longer related to the engagement force. When AWD vehicle drives on a homogeneous road surface while the transfer case clutch is in the fully lock-up state, the dynamic equation of motion for the wheel can be expressed as follows:

$$I_w\dot{\omega}_i = \left(\frac{l_r}{L} - \frac{a_x h}{gL}\right)\frac{T_t i_f}{2} - T_{bi} - R_e F_{xi} - R_e R_r F_{zi},\ i = 1, 2 \quad (6)$$

$$I_w\dot{\omega}_i = \left(\frac{l_f}{L} + \frac{a_x h}{gL}\right)\frac{T_t i_r}{2} - T_{bi} - R_e F_{xi} - R_e R_r F_{zi},\ i = 3, 4 \quad (7)$$

where L is the wheel base length and h is the height from ground to vehicle's center of gravity (CG). Due to the intrinsic hardware structure of the transfer case, allowable engagement force is constrained in AWD vehicle.

2.3. Tire Model

2.3.1. Steady-state tire model

With the proper tire parameters and tire sideslip angle, the steady-state lateral tire force is described as follows:

$$\bar{F}_{yi} = C_\alpha \alpha_i,\ i = 1, 2, 3, 4 \quad (8)$$

where C_α is the cornering stiffness and α_i is the wheel sideslip angle.

2.3.2. Dynamic tire model

Because of the characteristics of the tire material, tire forces generated exhibit a lagging behavior, especially in the lateral direction. The dynamic lateral tire force can be expressed as a first order dynamic equation:

$$\frac{\sigma}{v_x}\dot{F}_{yi} + F_{yi} = \bar{F}_{yi},\ i = 1, 2, 3, 4 \quad (9)$$

where σ is the relaxation length, which consists of three tire characteristic parameters. It can be expressed as follows (Lee *et al.*, 2016):

$$\sigma = \left(\frac{C_\alpha^3}{K_L^3} - \frac{3C_\alpha K_D}{K_L^2}\right)^{\frac{1}{3}} \quad (10)$$

where K_L and K_D are the tire lateral stiffness and distortion stiffness.

3. TARGET STATES SELECTION FOR THE AWD CONTROLLER

3.1. Longitudinal Direction

It has been empirically proven that the tire-road friction

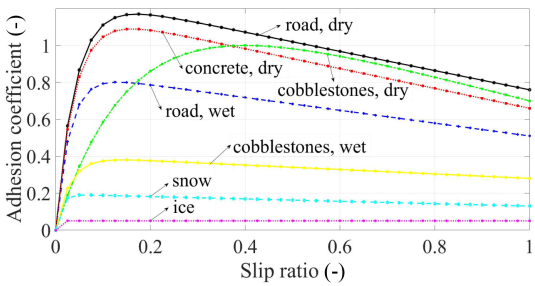

Figure 2. Typical adhesion coefficient characteristics.

coefficient is highly related to the wheel slip ratio (Burckhardt, 1993; Pacejka, 2012). Figure 2 shows the typical adhesion coefficient characteristics that are obtained from the Burckhardt's tire friction model. Except for extraordinary cases (e.g., dry cobblestone), the tire-road friction has a peak value at a certain wheel slip ratio for each road surface.

The wheel slip ratio, λ, is defined as follows:

$$\lambda = \begin{cases} \dfrac{R_e\omega - v_x}{R_e\omega}, \ acceleration \\ \dfrac{v_x - R_e\omega}{v_x}, \ deceleration \end{cases} \tag{11}$$

In the case of acceleration, the desired vehicle longitudinal velocity $v_{x,d}$, is obtained as follows:

$$v_{x,d} = R_e\omega(1-\lambda_d) \tag{12}$$

Using the CAN signal information, the wheel slip ratio can be obtained from the estimation algorithm for vehicle velocity. Therefore, wheel-slip-based control in the longitudinal direction is feasible without requiring additional sensors. Although each surface has a slightly different peak point, it was assumed that the desired wheel slip ratio was already known because the peak points are clustered at certain boundaries, and the purpose of this study was the control, not the desired target value generation. In this study, $\lambda_d = 0.15$ was used as the desired slip ratio.

3.2. Lateral Direction

Figure 3 shows the variation in the lateral motion of AWD vehicle depending on the transfer case engagement force during a double lane change. Open loop simulation results showed that the stronger the engagement force, the smaller the sideslip angle and yaw rate, which validated that the AWD system helped the vehicle to have stable lateral motion. As for the target of lateral motion states, the sideslip angle β and yaw rate γ have been selectively used in previous studies. Control based on yaw rate only has been widely adopted in most of the previous studies because the yaw rate sensor is built into the vehicle. Although control based on both the yaw rate and sideslip angle can further improve the lateral stability of vehicle, it requires additional estimator or sensor. Also, an AWD system distributes the engine torque just between front and rear, not side to side, which limits lateral dynamic responsiveness. Therefore, this study adopted yaw rate only as a target state for vehicle lateral stability.

The desired yaw rate γ_d, which indicates the vehicle in steady-state cornering is expressed as follows:

$$\gamma_d = \mathrm{sgn}(\delta_f)\max\left(\left|\frac{|v_x\delta_f|}{L+\frac{mv_x^2}{L}\left(\frac{l_r}{C_f}-\frac{l_f}{C_r}\right)}\frac{1}{\frac{\sigma}{v_x}s+1}\right|, \left|\frac{\mu g}{v_x}\right|\right) \tag{13}$$

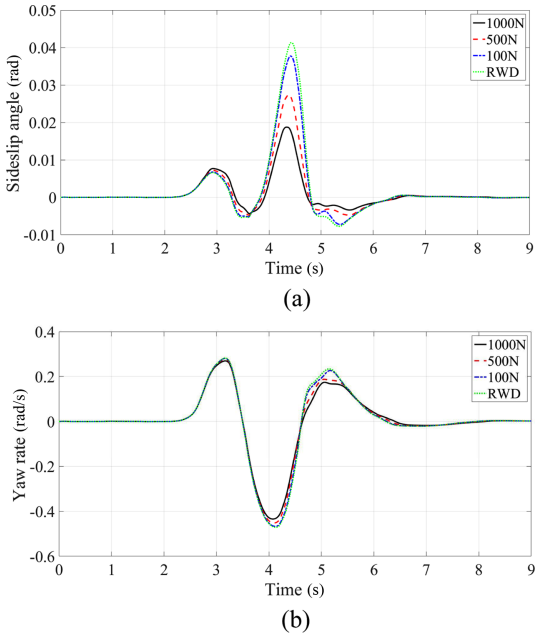

Figure 3. Variation of vehicle lateral motion depending on the transfer case engagement force during double lane change ($\mu = 0.9$): (a) Sideslip angle; (b) Yaw rate.

where C_f and C_r are the front and rear cornering stiffnesses, respectively. Conventional approaches have not considered the effects of AWD system to the vehicle lateral stability improvement. By adopting planar full car model that is introduced in third section, this study suggests the AWD controller that simultaneously considers both longitudinal and lateral motions.

4. VEHICLE MODEL FOR CONTROLLER APPLICATION

Selecting proper vehicle model for controller design is important since it is closely related to the performance of the controller. In previous studies of vehicle dynamics controller design, a bicycle model with a yaw moment term was most frequently used. However, this bicycle model is inappropriate for an AWD controller because the relationship between the transfer case engagement force (control input) and states is not adequately represented. Since the transfer case control input term appears in the wheel dynamics model, it should be included in the entire model for control applications. The wheel dynamics model is related to other models through tire forces so it is necessary to construct a vehicle model based on the tire forces. Therefore, the following planar full car model of (14), which represent the relationship between the control input and states explicitly, was adopted for the control application:

$$\begin{bmatrix} \dot{v}_x \\ \dot{v}_y \\ \dot{\gamma} \\ \dot{\omega}_1 \\ \dot{\omega}_2 \\ \dot{\omega}_3 \\ \dot{\omega}_4 \\ \dot{\mathbf{F}}_{x[4\times1]} \\ \dot{\mathbf{F}}_{y[4\times1]} \end{bmatrix} = \begin{bmatrix} \frac{1}{m}\{(F_{x1}+F_{x2})\cos(\delta_f)-(F_{y1}+F_{y2})\sin(\delta_f)+\cdots \\ F_{x3}+F_{x4}-\rho_{air}C_d A v_x^2/2\}+v_y\gamma \\ \frac{1}{m}\{(F_{x1}+F_{x2})\sin(\delta_f)+(F_{y1}+F_{y2})\cos(\delta_f)+\cdots \\ F_{y3}+F_{y4}\}-v_x\gamma \\ \frac{1}{I_z}\Big[l_f\{(F_{x1}+F_{x2})\sin(\delta_f)+(F_{y1}+F_{y2})\cos(\delta_f)\}+\cdots \\ t_w\{(-F_{x1}+F_{x2})\cos(\delta_f)+(F_{y1}-F_{y2})\cos(\delta_f)-\cdots \\ F_{x3}+F_{x4}\}-l_r(F_{y3}+F_{y4})\Big] \\ \frac{1}{I_w}\left(\mu_c r_c F_c \frac{i_f}{2}-T_{b1}-R_e F_{x1}-R_e R_r F_{z1}\right) \\ \frac{1}{I_w}\left(\mu_c r_c F_c \frac{i_f}{2}-T_{b2}-R_e F_{x2}-R_e R_r F_{z2}\right) \\ \frac{1}{I_w}\left\{(T_t-\mu_c r_c F_c)\frac{i_f}{2}-T_{b3}-R_e F_{x3}-R_e R_r F_{z3}\right\} \\ \frac{1}{I_w}\left\{(T_t-\mu_c r_c F_c)\frac{i_f}{2}-T_{b4}-R_e F_{x4}-R_e R_r F_{z4}\right\} \\ \mathbf{0}_{[4\times1]} \\ \frac{v_x}{\sigma}(-\mathbf{F}_{y[4\times1]}+\bar{\mathbf{F}}_{y[4\times1]}) \end{bmatrix} \tag{14}$$

Here, the front wheel steering angles are assumed to be equal, i.e., $\delta_f = \delta_1 = \delta_2$.

Linearizing (14), the following state-space form is obtained:

$$\dot{x} = A_l x + B_l F_c + E_l \tag{15}$$

where $x = [v_x, v_y, \gamma, \omega_{[1\times4]}, \mathbf{F}_{[1\times8]}]^T$, $\omega_{[1\times4]} = [\omega_1, \omega_2, \omega_3, \omega_4]$ and $\mathbf{F}_{[1\times8]} = [F_{x1}, F_{x2}, F_{x3}, F_{x4}, F_{y1}, F_{y2}, F_{y3}, F_{y4}]$. A_l, B_l, and E_l are defined in (16), (17), and (18).

5. PHYSICAL CONSTRAINTS IN AN AWD VEHICLE

An AWD vehicle has constraints that are determined by its actual hardware structure and external conditions and which should be considered when designing a controller.

5.1. Input Constraints

In the lock-up state, the amount of driving torque distributed to the front and rear wheels is no longer determined by the clutch engagement force, such that additional engagement force cannot affect the change of motion of the vehicle. Therefore, the controller should be designed so that the upper bound of the control input be the engagement force that turns the AWD system to the lock-up state. Assuming that the front and rear final reduction gear ratios and front and rear wheel radii are the same, when AWD vehicle drives on a homogeneous road surface while the transfer case clutch is in the fully lock-up state, the clutch engagement force is bounded as follows:

$$A_l = \begin{bmatrix} \frac{-\rho_{air}C_d A}{m} & \gamma & v_y & & \frac{\cos(\delta_f)}{m} & \frac{\cos(\delta_f)}{m} \\ -\gamma & 0 & -v_x & \mathbf{0}_{[3\times4]} & \frac{\sin(\delta_f)}{m} & \frac{\sin(\delta_f)}{m} \\ 0 & 0 & 0 & & \frac{l_f\sin(\delta_f)-t_w\cos(\delta_f)}{I_z} & \frac{l_f\sin(\delta_f)+t_w\cos(\delta_f)}{I_z} \\ & & & \mathbf{0}_{[4\times7]} & & \frac{-R_e}{I_w}\cdot\mathbf{I}_{[4\times4]} \\ & & & & & \mathbf{0}_{[4\times15]} \\ & & \frac{-\mathbf{F}_y+\bar{\mathbf{F}}_y}{\sigma}\cdot\mathbf{I}_{[4\times4]} & & & \mathbf{0}_{[4\times7]} \end{bmatrix}$$

$$\begin{bmatrix} \frac{1}{m} & \frac{1}{m} & -\frac{\sin(\delta_f)}{m} & -\frac{\sin(\delta_f)}{m} & 0 & 0 \\ 0 & 0 & \frac{\cos(\delta_f)}{m} & \frac{\cos(\delta_f)}{m} & \frac{1}{m} & \frac{1}{m} \\ \frac{-t_w}{I_z} & \frac{t_w}{I_z} & \frac{l_f\cos(\delta_f)+t_w\sin(\delta_f)}{I_z} & \frac{l_f\cos(\delta_f)+t_w\sin(\delta_f)}{I_z} & \frac{-l_r}{I_z} & \frac{-l_r}{I_z} \\ & & & \mathbf{0}_{[4\times4]} & & \\ & & & \frac{-v_x}{\sigma}\cdot\mathbf{I}_{[4\times4]} & & \end{bmatrix} \tag{16}$$

$$B_l = \left[\mathbf{0}_{[1\times3]} \ \frac{\mu_c r_c i_f}{2I_w} \ \frac{\mu_c r_c i_f}{2I_w} \ -\frac{\mu_c r_c i_r}{2I_w} \ -\frac{\mu_c r_c i_r}{2I_w} \ \mathbf{0}_{[1\times4]} \ \mathbf{0}_{[1\times4]}\right]^T \tag{17}$$

$$E_l = \left[\mathbf{0}_{[1\times3]} \ -\frac{R_e R_{r1}}{I_w} \ -\frac{R_e R_{r2}}{I_w} \ \frac{T_t i_r}{2I_w} \ -\frac{R_e R_{r3}}{I_w} \ \frac{T_t i_r}{2I_w} \ -\frac{R_e R_{r4}}{I_w} \ \mathbf{0}_{[1\times4]} \ \mathbf{0}_{[1\times4]}\right]^T \tag{18}$$

$$0 \le F_c \le \left(\frac{l_r}{L}-\frac{a_x h}{gL}\right)\frac{T_t}{\mu_c r_c} \tag{19}$$

5.2. State Constraints

5.2.1. Yaw rate

Regardless of the type of vehicle drivetrain, the yaw rate, one of the vehicle motion states and the principal state for evaluating the lateral response of the vehicle, has a lower and upper limit that is determined by an external condition. Thus, it should be considered for controller design. The yaw rate limit is expressed as follows:

$$|\gamma| \le \left|\frac{F_{y,\max}}{mv_x}\right| \approx \left|\frac{\mu F_z}{mv_x}\right| = \left|\frac{\mu g}{v_x}\right| \tag{20}$$

5.2.2. Tire force

For the same reason as the yaw rate state, the tire force is lower and upper-bounded by an external condition. The bounded condition of tire force at each wheel is expressed as follows:

$$|F_{xi}| \le \mu F_{zi}, \ i = 1, 2, 3, 4 \tag{21}$$

$$|F_{yi}| \le \mu F_{zi}, \ i = 1, 2, 3, 4 \tag{22}$$

6. MPC CONTROLLER DESIGN

6.1. MPC Algorithm

Given the process model and current states, the MPC calculates a set of optimal inputs that minimize the cost function while satisfying the input and states constraints over a predetermined prediction time horizon at each step. Then, only the first input in the set of optimal inputs is used because a set of optimal inputs is newly obtained in each step with the updated values of the vehicle states. To formulate the MPC problem, a process model in discretized form is required. For the MPC-based AWD controller design, (15) was discretized using a zero-order hold as follows:

$$x_{k+1} = A_k x_k + B_k u_k + E_k \tag{23}$$

where $u_k = F_{c,k}$.

Then, the cost function of the MPC in quadratic form is defined as follows:

$$J(x_k, U_k) = \sum_{i=0}^{N-1} \left\{ (x_{k+i} - x_{d,k+i})^T Q (x_{k+i} - x_{d,k+i}) + \cdots \right. \\ \left. u_{k+i}^T R u_{k+i} \right\} + (x_{k+N} - x_{d,k+N})^T P (x_{k+N} - x_{d,k+N}) \tag{24}$$

where

$$U_k = \left[u_k, u_{k+1}, \cdots, u_{k+N-1} \right]^T \tag{25}$$

The predicted state sequence obtained by the discretized process model (23) with the input sequence U_k can be expressed as:

$$X_k = L^x x_k + L^u U_k + L^e \tag{26}$$

where

$$X_k = \begin{bmatrix} x_{k+1} \\ x_{k+2} \\ \vdots \\ x_{k+N} \end{bmatrix}, \; L^x = \begin{bmatrix} A_k \\ A_k^2 \\ \vdots \\ A_k^N \end{bmatrix},$$

$$L^u = \begin{bmatrix} B_k & 0 & \cdots & \cdots & 0 \\ A_k B_k & B_k & & & 0 \\ \vdots & \vdots & \ddots & & \\ \vdots & \vdots & & \ddots & \\ A_k^{N-1} B_k & A_k^{N-2} B_k & \cdots & \cdots & B_k \end{bmatrix},$$

$$L^e = \begin{bmatrix} E_k \\ A_k E_k + E_k \\ \vdots \\ A_k^{N-1} E_k + \cdots + E_k \end{bmatrix}$$

Using X_k and U_k and removing the terms that are not related to U_k, the cost function is compactly expressed as follows:

$$J(x_k, U_k) = X_k^T \bar{Q} X_k + U_k^T \bar{R} U_k - 2 X_{d,k}^T \bar{Q} X_k \tag{27}$$

where

$$\bar{Q} = blockdiag\left[Q, \cdots, Q, P \right] \\ \bar{R} = blockdiag\left[R, \cdots, R \right] \\ X_{d,k} = \left[x_{d,k}, x_{d,k+1}, \cdots, x_{d,k+N} \right]^T \tag{28}$$

The cost function used in the calculation of the optimal control input is affected by the values of matrices Q and R. Although the MPC helps the AWD system respond preemptively, the constant values of the matrices do not actively address the time-variable situation of the vehicle. By setting target errors to be included in the matrix Q, the MPC can be designed to respond more sensitively to the target error. The values of Q and R that were used in this study is defined as follows:

$$Q = \begin{cases} diag\left[\left(1 + \max(abs(\lambda) - abs(\lambda_d), 0) \right) \cdot 10^9 \cdot 5.01 \cdot \mathbf{1}_{[1\times 14]} \right] \\ \quad if \;\; abs(\lambda_d) \geq 0.035 \;\&\; abs(\lambda) - abs(\lambda_d) \\ diag\left[\left(3.16 \cdot 10 \cdot \dfrac{\lambda_1 + \lambda_2}{2} + 1 \right) \cdot 3.16 \cdot 10^3 \cdot 5.01 \cdot \mathbf{1}_{[1\times 14]} \right] \\ \quad else \end{cases} \\ R = 1 \tag{29}$$

Here $\mathbf{1}$ is the vector of which each component is 1. Substituting (24) into (25), the cost function is rewritten as follows:

$$J(x_k, U_k) = (L^x x_k + L^u U_k + L^e)^T \bar{Q} (L^x x_k + L^u U_k + L^e) + \cdots \\ U_k^T \bar{R} U_k - 2 X_{d,k}^T \bar{Q} (L^x x_k + L^u U_k + L^e) \tag{30}$$

Finally, dropping the terms that are not related to U_k, (27) is simplified as follows:

$$J(x_k, U_k) = U_k^T \left\{ (L^u)^T \bar{Q} L^u + \bar{R} \right\} U_k + \cdots \\ 2 \left\{ x_k^T (L^x)^T \bar{Q} L^u + (L^e)^T \bar{Q} L^u - X_{d,k}^T \bar{Q} L^u \right\} U_k \tag{31}$$

6.2. Incorporating Constraints

To obtain the optimal control input that minimizes the cost function (31) given system constraints, all constraints should be rearranged as inequalities of U_k. Assuming that the system input and states are bounded, the sequence of U_k and X_k are expressed as follows:

$$\underline{u} \leq U_k \leq \bar{u} \tag{32}$$

$$\underline{x} \leq X_k \leq \bar{x} \tag{33}$$

Then, (30) is rearranged as follows:

$$\begin{bmatrix} I_{N\times N} \\ -I_{N\times N} \end{bmatrix} U_k \leq \begin{bmatrix} I_{N\times 1} \bar{u} \\ -I_{N\times 1} \underline{u} \end{bmatrix} \tag{34}$$

Using (24), (31) is rewritten as related by U_k:

$$\begin{bmatrix} L_i^u \\ -L_i^u \end{bmatrix} U_k \leq \begin{bmatrix} \bar{x} \\ \underline{x} \end{bmatrix} + \begin{bmatrix} -A_k^i \\ A_k^i \end{bmatrix} x_k + \begin{bmatrix} -L_i^e \\ L_i^e \end{bmatrix}, \; i = 1, 2, \cdots, N \tag{35}$$

where L_i^u and L_i^e are i^{th} block row of L^u and L^e,

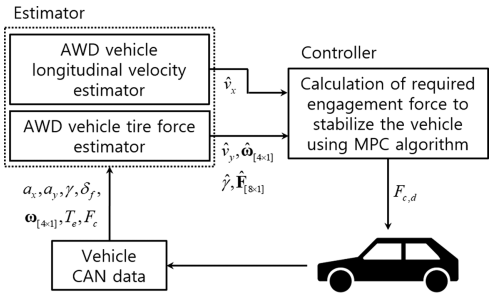

Figure 4. Diagram of the model-based AWD controller.

respectively. Finally, the states and input constraints are merged together to be represented as one matrix form of inequality:

$$A_c U_k \le b_x + B_x x_k \tag{36}$$

where

$$A_c = \begin{bmatrix} I_{[N\times N]} \\ -I_{[N\times N]} \\ L^u \\ -L^u \end{bmatrix}, b_x = \begin{bmatrix} I_{[N\times 1]}\overline{u} \\ -I_{[N\times 1]}\underline{u} \\ \overline{x}_{[n\times 1]} + L_i^e \\ -\underline{x}_{[n\times 1]} - L_i^e \end{bmatrix}, B_x = \begin{bmatrix} \mathbf{0}_{[n\times N]} \\ \mathbf{0}_{[n\times N]} \\ -A_k^i \\ A_k^i \end{bmatrix} \tag{37}$$

where n is the degree of freedom of the system. The MPC problem is then defined to find the solution for the optimal control inputs that minimize the cost function (29) subject to the constraints of (34):

$$\min_U \; U_k^T \left\{ (L^u)^T \bar{Q} L^u + \bar{R} \right\} U_k + \cdots$$
$$2\left\{ x_k^T (L^x)^T \bar{Q} L^u + (L^e)^T \bar{Q} L^u - X_{d,k}^T \bar{Q} L^u \right\} U_k \tag{38}$$

$$\text{subject to } A_c U_k \le b_x + B_x x_k$$

7. SIMULATION RESULTS AND ANALYSIS

To validate the proposed controller, simulations were conducted using CarSim. The simulation environment for the AWD vehicle was constructed by implementing the transfer case plant model developed with Simulink as the external model. The vehicle driveline is front engine, rear wheel drive (FR) type, for which the installation of an AWD system is greatly needed. Figure 4 shows the overall structure of the controller. The proposed planar full car model-based controller requires the information for the tire force at each wheel. Therefore, the tire force estimation process should be included. This study adopted a tire force estimator for an AWD vehicle that is designed by Jung and Choi (2018). The current vehicle longitudinal velocity should also be estimated accurately to improve the performance of the AWD controller. Among several methods, a practical vehicle velocity estimation that requires no additional sensors was adopted in this study (Han *et al.*, 2017). The controller sampling time, T_s, was set

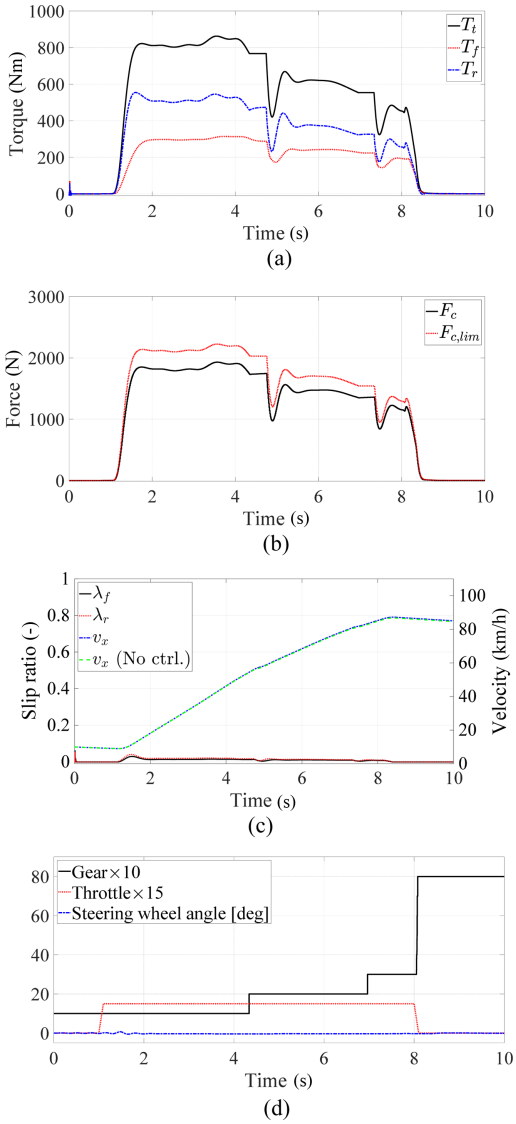

Figure 5. Rapid acceleration w/o steering on a normal road (μ = 0.85): (a) Front and rear driveshaft torque; (b) Clutch engagement force; (c) Front and rear slip ratio and longitudinal velocity; (d) Vehicle inputs.

to 10 ms. Prediction span for the MPC was set to 0.15 s (15 steps). Two simulation scenarios were selected. The first involved rapid acceleration without steering on both normal and slippery road. In this scenario, significant longitudinal slip occurs at the rear wheels, making it appropriate for the longitudinal traction validation. The second was rapid acceleration with a double lane change on a low-μ surface. Because this scenario causes a generation of large sideslip angle in RWD vehicle, it is appropriate for the lateral stability validation. To find out the local minimum of vector-valued quadratic function that includes bounded condition in the variable, *quadprog* solvers, which is provided in MATLAB, was used. Table A.1 in Appendix shows specifications of the vehicle.

7.1. Rapid Acceleration without Steering

The first test of the simulation was rapid acceleration without steering. The vehicle started to accelerate rapidly (full throttle) at t = 1s with an initial velocity of 10 km/h (see Figure 5 (d)). Figure 5 shows the test results of the MPC-based controller on a normal road. Although a large amount of throttle input was added, significant wheel slip was not generated at either wheel (see the red dotted and solid black lines of Figure 5 (c)). More specifically, a wheel slip of approximately 0.05 was generated initially at each wheel and diminished to zero as the vehicle accelerated and gear upshift occurred. Although vehicle wheel slip greater than desired value was not generated, the MPC-based controller commanded the transfer case clutch to actuate with a high engagement force which was slightly lower than its limit (see Figure 5 (b)) while the vehicle is accelerating. This simulation result shows the preemptive characteristic of MPC-based controller operation to prevent any substantial wheel slip, which is different from PID control. However, on normal road, there were no much big difference of acceleration performance between vehicle with MPC and that without control. Figure 5 (a) shows the front and rear shaft torques that were distributed at both wheels.

Figure 6 shows the simulation result of the MPC-based controller on a slippery road. The vehicle inputs were the same as in the normal road case (see Figure 6 (d)). Initially, the MPC-based controller commanded the transfer case clutch to be strongly engaged, but large slips occurred at the rear wheels owing to the limit of the road condition (see the red dotted line of Figure 6 (c)).

Figure 6 (b) shows the clutch engagement force of AWD system. Here, controller maintained the engagement force near its limit while the wheel slip was generated. Although

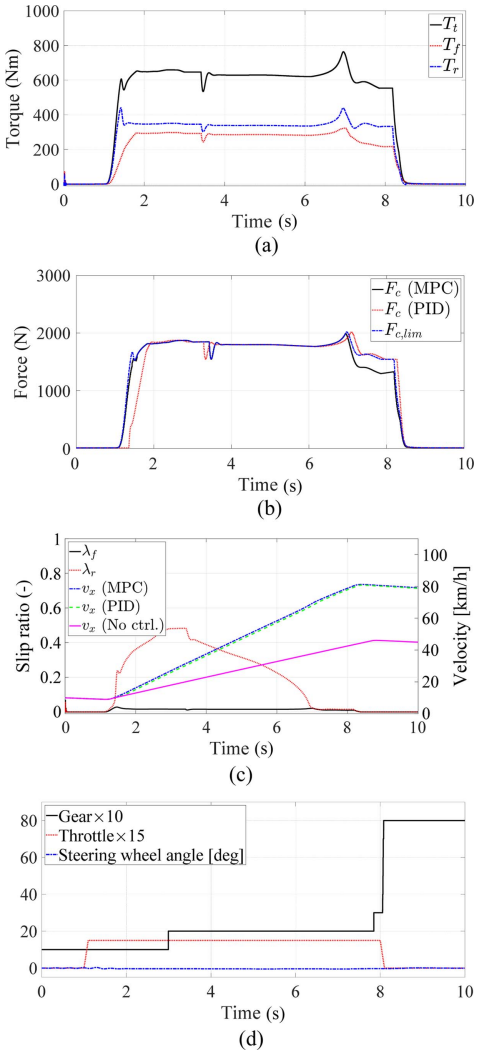

Figure 6. Rapid acceleration w/o steering on a slippery road (μ = 0.3): (a) Front and rear driveshaft torque; (b) Clutch engagement force; (c) Front and rear slip ratio and longitudinal velocity; (d) Vehicle inputs.

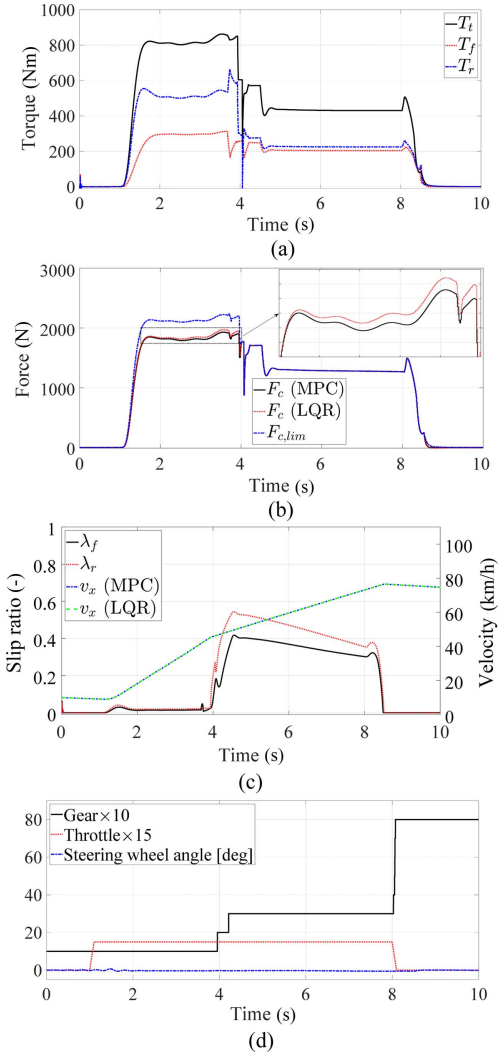

Figure 7. Rapid acceleration w/o steering on a split-μ surface (μ = 0.85 to μ = 0.2): (a) Front and rear driveshaft torque; (b) Clutch engagement force; (c) Front and rear slip ratio and longitudinal velocity; (d) Vehicle inputs.

PID controller showed a quite similar response with MPC-based controller, PID controller inevitably included a lagged behavior of engagement there were force at the moment of initial acceleration.

Therefore, quite big difference of acceleration performance among vehicle with MPC, that with PID control, and that without control.

Figure 7 shows the test results of the MPC-based controller on a split-μ surface. On a high-μ surface, there were no large amount of wheel slip at both wheels (see t = 1 ~ 4 s of Figure 7 (c)), and the proposed controller commanded the transfer case clutch to hold an engagement force that is lower than its limit. However, there appeared large amount of wheel slips at both wheels when vehicle enters into the low-μ surface (see t = 4 ~ 8 s of Figure 7 (c)), and the controller instantaneously commanded the transfer case clutch to hold an engagement force as its limit. Figure 7 (a) shows the front and rear shaft torques that were distributed to both wheels and Figure 7 (d) shows the vehicle inputs. Figure 7 (b) shows the clutch engagement force of both MPC and LQR controller. On high-μ surface there was a certain difference of clutch engagement force However, they became equal when vehicle enters into low-μ surface because of the large wheel slip caused engagement force to be persisted at its limit. More specifically, LQR control showed slightly higher engagement force on high-μ because system constraints are omitted in LQR scheme. Although there appeared some different response of clutch engagement force, acceleration performances between them were not remarkable. However, the accumulation of small slip difference may be significant in a long term scale.

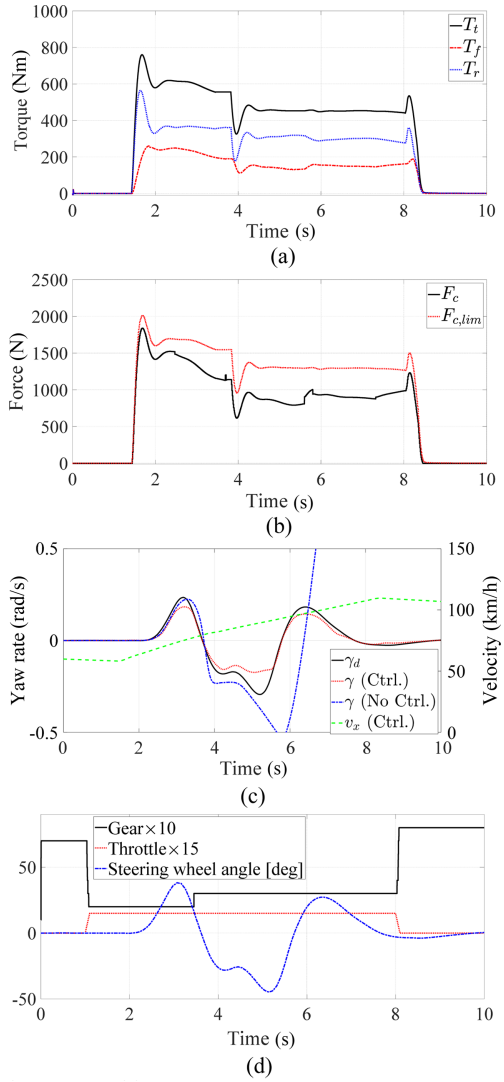

Figure 8. Rapid acceleration with double lane change on a slippery road (μ = 0.5): (a) Front and rear driveshaft torque; (b) Clutch engagement force; (c) Yaw rate; (d) Vehicle inputs.

7.2. Rapid Acceleration with Double Lane Change

The final test of the simulation involved rapid acceleration with a double lane change on a slippery road. In this scenario, while the vehicle was running at a constant velocity of 60 km/h, a rapid throttle input occurred just before maneuvering (see Figure 8 (d)). As expected, the RWD vehicle spun out on the road. However, the AWD vehicle could negotiate the double lane change motion, with the proper clutch engagement force from transfer case (see Figures 8 (a) and (b)). Similar to previous simulations, the engagement force initially reached the limit, then gradually decreased. Although the transfer case was not fully engaged, the AWD vehicle could almost follow the desired yaw rate, γ_d (see Figure 8 (c)). Also, due to the time-varing value of Q, the engagement force was changed slightly depending on the current vehicle status (see Figure 8 (b)).

8. CONCLUSION

This paper proposed a model-based controller for an AWD vehicle. Considering the constrained characteristics of the AWD system, MPC method that can calculate the optimal control input while simultaneously concerning input and state constraints was selected for the advanced AWD controller design. In driving scenarios that is able to cause the vehicle to have a slow or an unstable response in both longitudinal and lateral directions, the proposed controller helped the vehicle have a fast and a stable response. More specifically, the MPC-based controller showed better longitudinal acceleration performance than PID controller, especially when the vehicle is driving on slippery road. With the preemptive characteristic of MPC algorithm, the suggested controller can deal with various road conditions without having oscillations or lagged behavior of control input, which cannot be solved by PID controller. Also, the MPC-based controller showed a little bit conservative response of clutch engagement force than the LQR controller due to the condition of system constraints. Also,

the suggested controller provided optimal clutch engagement force that makes AWD vehicle has stable lateral response only with front to rear torque distribution when there is a possibility of vehicle spin-out. Although the proposed algorithm was verified by an AWD vehicle simulation model integrated with commercial software, there may be other considerations for a real vehicle experiment. For instance, input constraints could be changed depending on whether the transfer case clutch is in a slipping or lock-up states. Also, a robust control scheme that effectively mitigates the errors due to model uncertainties should be considered in future studies.

ACKNOWLEDGEMENT–This work was partly supported by the National Research Foundation of Korea (NRF) grant funded by the Korea government (MSIP) (No. 2017R1A2B4004116), and the BK21+ program through the NRF funded by the Ministry of Education of Korea.

REFERENCES

Borrelli, F., Bemporad, A. and Morari, M. (2017). *Predictive Control for Linear and Hybrid Systems*. Cambridge University Press. Cambridge, UK.

Burckhardt, M. (1993). *Fahrwerktechnik, Radschlupf-Regelsysteme*. Vogel Fachbuch. Würzburg, Germany.

Camacho, E. F. and Bordons, C. (2007). *Model Predictive Control*. 2nd edn. Springer-Verlag London. London, UK.

Choi, S. B. (2008). Antilock brake system with a continuous wheel slip control to maximize the braking performance and the ride quality. *IEEE Trans. Control System Technology* **16**, **5**, 996–1003.

Choi, M. and Choi, S. B. (2014). Model predictive control for vehicle yaw stability with practical concerns. *IEEE Trans. Vehicular Technology* **63**, **8**, 3539–3548.

Choi, M. and Choi, S. B. (2016). MPC for vehicle lateral stability via differential braking and active front steering considering practical aspects. *Proc. Institution of Mechanical Engineers, Part D: J. Automobile Engineering* **230**, **4**, 459–469.

Croft-White, M. and Harrison, M. (2006). Study of torque vectoring for all-wheel-drive vehicles. *Vehicle System Dynamics: Int. J. Vehicle Mechanics and Mobility* **44**, **Supplement 1**, 313−320.

Han, K., Lee, E., Choi, M. and Choi, S. B. (2017). Adaptive scheme for the real-time estimation of tire-road friction coefficient and vehicle velocity. *IEEE/ASME Trans. Mechatronics* **22**, **4**, 1508−1518.

Jalali, M., Khajepour, A., Chen S.-k. and Litkouhi, B. (2017). Handling delays in yaw rate control of electric vehicles using model predictive control with experimental verification. *J. Dynamic Systems, Measurement, and Control* **139**, **12**, 121001.

Jung, H. and Choi, S. (2016). Control of awd system for vehicle performance and safety. *MATEC Web of Conf.*, **56**, 06004.

Jung, H. J. and Choi, S. B. (2018). Real-time individual tire force estimation for an all-wheel drive vehicle. *IEEE Trans. Vehicular Technology* **67**, **4**, 2934–2944.

Kim, H., Lee, S. and Hedrick, J. K. (2015). Active yaw control for handling performance improvement by using traction force. *Int. J. Automotive Technology* **16**, **3**, 457–464.

Lee, E., Lee, J. and Choi, S. (2016). String tire model for evaluating steering agility performance using tire cornering force and lateral static characteristics. *Vehicle System Dynamics: Int. J. Vehicle Mechanics and Mobility* **55**, **2**, 231−243.

Nam, K., Fujimoto, H. and Hori, Y. (2012). Lateral stability control of inwheel-motor-driven electric vehicles based on sideslip angle estimation using lateral tire force sensors. *IEEE Trans. Vehicular Technology* **61**, **5**, 1972–1985.

Osborn, R. P. and Shim, T. (2006). Independent control of all-wheel-drive torque distribution. *Vehicle System Dynamics: Int. J. Vehicle Mechanics and Mobility* **44**, **7**, 529–546.

Pacejka, H. (2012). *Tire and Vehicle Dynamics*. 3rd edn. Butterworth-Heinemann. Oxford, UK.

Rajamani, R. (2012). *Vehicle Dynamics and Control*. 2nd edn. Springer. New York, USA.

Williams, R. C. (2006). 4WD-AWD market trends in vehicles and technology differences and similarities, from 1997 to 2004 primarily in the US market, and also some global comparisons. *SAE Paper No*. 2006-01-0822.

Yoon, J., Cho, W., Koo, B. and Yi, K. (2009). Unified chassis control for rollever prevention and lateral stability. *IEEE Trans. Vehicular Technology* **58**, **2**, 596–609.

APPENDIX

Table A.1. Vehicle specifications.

Parameter	Value
Distance from CG to front and rear axle, l_f, l_r	1.471 m, 1.539 m
Height from ground to CG, h	0.54 m
Front and rear track width, $2t_w$	1.63 m
Effective wheel radius, R_e	0.328 m
Vehicle total mass, m	2050 kg
Vehicle moment of inertia about yaw axis, I_z	4200 kg m^2
Wheel moment of inertia, I_w	0.9 kg m^2
Final reduction gear ratio of front and rear, i_f, i_r	43/11, 43/11
Rolling resistance, R_r	0.015